HHS Public Access

Author manuscript

ACS Nano. Author manuscript; available in PMC 2023 April 27.

Published in final edited form as:

ACS Nano. 2021 October 26; 15(10): 15741–15753. doi:10.1021/acsnano.0c09553.

Brain-Accumulating Nanoparticles for Assisting Astrocytes to Reduce Human Immunodeficiency Virus and Drug Abuse-Induced Neuroinflammation and Oxidative Stress

Bapurao Surnar,
Department of Biochemistry and Molecular Biology, University of Miami Miller School of Medicine, Miami, Florida 33136, United States

Anuj S. Shah,
Department of Biochemistry and Molecular Biology, University of Miami Miller School of Medicine, Miami, Florida 33136, United States

Minseon Park,
Department of Biochemistry and Molecular Biology, University of Miami Miller School of Medicine, Miami, Florida 33136, United States

Akil A. Kalathil,
Department of Biochemistry and Molecular Biology, University of Miami Miller School of Medicine, Miami, Florida 33136, United States

Mohammad Z. Kamran,
Department of Biochemistry and Molecular Biology, University of Miami Miller School of Medicine, Miami, Florida 33136, United States

Royden Ramirez Jaime,
Department of Immunology and Nano-Medicine, Herbert Wertheim, College of Medicine, Florida International University, Miami, Florida 33199, United States

Michal Toborek,
Department of Biochemistry and Molecular Biology, University of Miami Miller School of Medicine, Miami, Florida 33136, United States

Madhavan Nair,

Corresponding Authors: Nagesh Kolishetti – Department of Immunology and Nano-Medicine, Herbert Wertheim, College of Medicine, Florida International University, Miami, Florida 33199, United States; Institute of Neuroimmune Pharmacology, Herbert Wertheim College of Medicine, Miami, Florida 33199, United States; nkolishe@fiu.edu, Shanta Dhar – Department of Biochemistry and Molecular Biology, University of Miami Miller School of Medicine, Miami, Florida 33136, United States; Sylvester Comprehensive Cancer Center, Miller School of Medicine, University of Miami, Miami, Florida 33136, United State; shantadhar@med.miami.edu.

Author Contributions

S.D. and N.K. conceptualized the research; S.D., M.T., and N.K. designed the research, supervised experiments, and provided directions and S.D., M.T., M. N., and N.K. provided resources; B.S., A.S., M.Z.K., R.J.R., M.P., A.K., and N.K. performed the research; B.S., A.S., M.P., A.K., and N.K contributed reagents; B.S., A.S., M.Z.K., A.K., M.P., M.T., M.N., N.K., and S.D. analyzed the data. All authors discussed the results and commented on the manuscript; B.S., A.S., M.Z.K., A.K., M.P., N.K., and S.D. wrote the manuscript.

Complete contact information is available at: https://pubs.acs.org/10.1021/acsnano.0c09553

The authors declare no competing financial interest.

Department of Immunology and Nano-Medicine, Herbert Wertheim, College of Medicine, Florida International University, Miami, Florida 33199, United States

Nagesh Kolishetti,
Department of Immunology and Nano-Medicine, Herbert Wertheim, College of Medicine, Florida International University, Miami, Florida 33199, United States; Institute of Neuroimmune Pharmacology, Herbert Wertheim College of Medicine, Miami, Florida 33199, United States

Shanta Dhar
Department of Biochemistry and Molecular Biology, University of Miami Miller School of Medicine, Miami, Florida 33136, United States; Sylvester Comprehensive Cancer Center, Miller School of Medicine, University of Miami, Miami, Florida 33136, United States

Abstract

Human neurotropic immunodeficiency virus (HIV) ingress into the brain and its subsequent replication after infection results in viral reservoirs in the brain. The infected cells include microglia, perivascular macrophages, and astrocytes. HIV-associated neurocognitive disorders (HAND) affect glial cells by activating microglia and macrophages through neuroinflammation, as well as astrocytes through mitochondrial dysfunctions and the onset of oxidative stress, impairing the ability of these cells to engage in neuroprotection. Furthermore, the risk of neuroinflammation associated with HAND is magnified by recreational drug use in HIV-positive individuals. Most of the therapeutic options for HIV cannot be used to tackle the virus in the brain and treat HAND due to the inability of currently available combination antiretroviral therapies (ARTs) and neuroprotectants to cross the blood–brain barrier, even if the barrier is partially compromised by infection. Here, we report a strategy to deliver an optimized antiretroviral therapy combined with antioxidant and anti-inflammatory neuroprotectants using biodegradable brain-targeted polymeric nanoparticles to reduce the burden caused by viral reservoirs in the brain and tackle the oxidative stress and inflammation in astrocytes and microglia. Through *in vitro* coculture studies in human microglia and astrocytes as well as an *in vivo* efficacy study in an EcoHIV-infected, methamphetamine-exposed animal model, we established a nanoparticle-based therapeutic strategy with the ability to treat HIV infection in the central nervous system in conditions simulating drug use while providing enhanced protection to astrocytes, microglia, and neurons.

Graphical Abstract

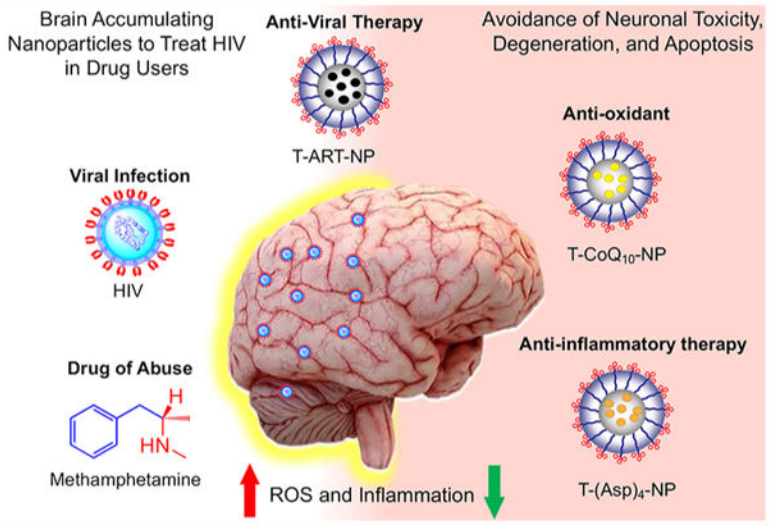

Keywords

reactive oxygen species; aspirin; mitochondrial dysfunction; efavirenz; darunavir; elvitegravir; coenzyme Q_{10}

The use of combination antiretroviral (ARV) therapy (cART) has changed the acute epidemic[1,2] of the human immunodeficiency virus (HIV) infections and acquired immunodeficiency syndrome (AIDS) into a chronic and treatable disease. More than ~690,000 people lose their lives from AIDS each year, and in 2019, 1.7 million people became newly infected with HIV. The hard-to-reach HIV reservoirs in the brain are often untreatable due to the inefficiency of CART in crossing the blood–brain barrier (BBB) to reach HIV-infected cells in the brain. Failure to treat these reservoirs often leads to severe neurological problems, named HIV-associated neurocognitive disorders (HAND), such as HIV dementia.[3,4] In addition, a large percentage of HIV-positive individuals abuse drugs such as methamphetamine (meth) and cocaine, which cause further oxidative stress by enhancing reactive oxygen species (ROS), mitochondrial dysfunctions, and inflammatory processes in HIV-infected areas in the brain.[5] Therefore, there is a growing need for ART not only to be delivered across the BBB but to be paired with antioxidant and/or anti-inflammatory neuroprotectants to alleviate HAND caused by both ART and drugs of abuse in the brains of HIV-positive individuals.[6–8] Although the precise underlying neuropathological mechanisms of HIV in humans are not completely understood, alterations in the function of glial cells such as astrocytes have been correlated with impaired neuronal function, including detrimental changes in synaptic function, neuronal polarity, axon and dendrite formation, and neuronal survival.[9–12] Furthermore, the activation of microglia and macrophages for neuroinflammation, the onset of mitochondrial dysfunction, and the formation of ROS in astrocytes impair the neuroprotective abilities of astrocytes.[13] Most of the therapeutic options, such as ART, that are meant to treat the brain viral reservoirs, as well as the neuroprotectants intended to tackle HAND, have limited efficacy due to the inability of the majority of these agents to cross the BBB, even when the barrier is partially

compromised by infection. A refined quality of life and overall survival for patients living with HIV infection urgently requires innovative modalities of combination treatments.

Nanoparticle (NP)-mediated delivery of cART and supplementation with antioxidant/anti-inflammatory-based neuroprotectants to the brain to improve neuronal functions for HIV and drug abuse patients with HIV conditions has not achieved its full potential. The delivery of cART and neuroprotectants to the brain can potentially be achieved by using biodegradable NPs engineered to achieve the following crucial milestones: (1) optimized size, charge, lipophilicity, and targeting properties to cross the BBB; (2) ability to reach the viral reservoirs and specific intracellular targets while demonstrating controlled release of the payload at the target; and (3) ameliorative effects on infected areas. This would enable effective and robust delivery of ARVs to the viral reservoirs and neuroprotectants to target cells such as astrocytes and microglia, to prevent neuronal degeneration. Thus, a highly lipophilic, biodegradable NP delivery platform with the ability to cross the BBB and deliver (1) ARVs to viral reservoirs of the brain, (2) antioxidants to the mitochondrial matrix of astrocytes rich in ROS, and (3) anti-inflammatory agents to the microglia of the brain can be extremely beneficial to show therapeutic effects and to control HAND in HIV-infected patients. In this work, we report that a combination of a brain-accumulating, mitochondrion-targeted, polymeric nanoparticle (T-NP) separately containing optimized combinatory ARVs, collectively abbreviated as T-ART-NPs or cART-NPs, a mitochondrion-acting antioxidant, coenzyme Q_{10} (CoQ_{10}), and a prodrug [Oc-G2-$(Asp)_4$] of an FDA-approved anti-inflammatory agent, aspirin, has the potential to provide therapeutic intervention against the viral load in the brain and tackle inflammation, oxidative stress, and mitochondrial dysfunction simultaneously in the presence of the virus and the recreational drug methamphetamine (meth) (Figure 1).

RESULTS AND DISCUSSION

Optimization of T-ARV-NPs.

We recently demonstrated that a self-assembled NP originating from a biocompatible block copolymer, poly(d,l-lactic-*co*-glycolic acid)-*block*-poly-(ethylene glycol)-triphenylphosphonium (PLGA-*b*-PEG-TPP), when blended with 10% TPP-$(CH_2)_5$-COOH, has the ability to cross the BBB based on *in vivo* studies conducted in small- and large-animal models as well as *in vitro* BBB models.[14] We first set out to optimize a library of ARV-loaded brain-accumulating NPs. As demonstrated in the previous study, the addition of 10% TPP-$(CH_2)_5$-COOH did not result in immunogenicity or toxicity from the NPs but did significantly improve uptake into the brain.[14] The initial loading of the 26 most widely used ARV drugs was tested in NPs of the targeted PLGA-*b*-PEG-TPP polymer at 20% feed of the drug with respect to the polymer (Table 1). The NPs were prepared using the conventional nanoprecipitation technique and purified by the ultracentrifugation method.[15–21] The Z-average hydrodynamic diameter and surface charge in terms of zeta potential of the NPs were measured using the dynamic light scattering (DLS) technique. The compiled data represented in Table 1 indicated that the diameter of the ARV-encapsulated NPs is in the range of 50–70 nm and the surface is positively charged. To test for the amount of drug loaded into the NPs, the NPs were subjected to high-performance liquid

chromatography (HPLC) along with free drug standards. Of the 26 drugs, only nine drugs, saquinavir (SQV), darunavir (DRV), elvitegravir (EVG), dolutegravir (DTG), raltegravir (RAL), bictegravir (BIC), efavirenz (EFV), delavirdine (DLV), and stavudine (d4T), showed signs of loading into the NPs (Table 1). Five of these drugs, DTG, RAL, DLV, BIC, and d4T, showed minimal loading. The four drugs that showed a higher percentage of loading were SQV, EFV, DRV, and EVG (Table 1). We then carried out further optimization of NPs on multiple fronts. First, we varied the %feed of ARVs to look for the best possible loading and encapsulation efficiency (EE) for a given drug in the NPs keeping the NP diameter below 100 nm and a zeta potential indicating a highly positive charged surface. Next, we investigated the stability of NPs with respect to drug release profiles. Typically, with these types of formulations, we could tune the drug release profiles from hours to days. Selected formulations were evaluated for drug release kinetics under physiological conditions of pH 7.4 at 37 °C. Our studies examined the %loading of nine different ARVs from four different categories: protease inhibitors (PI), which inhibit HIV's protease and final proteolytic cleavage of viral protein precursors; integrase inhibitors (INI), which prevent insertion of HIV viral genome into host cell DNA; and nucleoside and non-nucleoside reverse transcriptase inhibitors (NRTI, NNRTI), which block HIV's reverse transcriptase enzyme from converting viral RNA to DNA (Figure 2A). This was done by varying the percent feed from 10% to 50% and indicated that three drugs, EVF, EVG, and DRV, showed improved loading and NPs with good physicochemical properties (Figure 2B). Thus, we selected these three drugs to be incorporated in the T-NPs for potential application to tackle HIV under conditions of drugs of abuse. Since our optimization techniques resulted in good NP encapsulation of drug from each category, in this work, we also set out to investigate the effects of a combination of DRV, which is a PI, EVG, which is an INI, and EFV, which is an NNRTI (Figure 2A). Analysis of the morphology of the NPs encapsulated with these three drugs by transmission electron microscopy (TEM) indicated spherical, homogeneous particles (Figure 2C) complementing the diameter determined by the DLS technique. *In vitro* drug release studies in PBS (pH 7.4) at 37 °C indicated controlled release profiles of all three drugs from the respective NPs (Figure 2D).

Effects of ARVs and Drugs of Abuse on Cellular Health.

HIV-associated neurocognitive disorders affecting glia cells become worse when the HIV patients use drugs of abuse such as cocaine or meth. In addition, well-known ARVs also contribute to inflammation and oxidative stress to worsen the symptoms of HAND. For example, EFV has been shown to have effects in the central nervous system (CNS) such as dizziness, impaired concentration, and sleep disturbance. EFV can have damaging effects on neurons and microglia by altering calcium homeostasis, decreasing brain creatine kinase, and increasing pro-inflammatory cytokine levels, through mitochondrial damage. Changes in bioenergetics are likely caused by inhibition of mitochondrial complex IV of the electron transport chain (ETC). EVG is also associated with clinical psychiatric symptoms. EVG has been shown to have similar toXic effects on neurons and microglia, along with other side effects such as diarrhea. These toXic effects will potentially increase when an NP-based delivery approach is utilized, since with nanoparticle delivery of ARVs, these drugs are delivered specifically to the brain. Thus, by using aspirin- and CoQ_{10}-containing NPs along with ARV-NPs, these effects may be mitigated while keeping the drugs' antiretroviral

activity intact. We first checked the toXic effects of the ARVs which were loaded in the NPs at an appreciable amount. Microglia cells were treated with EFV, EVG, and DRV or the respective ARV-loaded NPs at various concentrations for 72 h. An MTT assay was conducted to test toXicity levels and calculate IC_{50} values (Figure S1). The MTT assay revealed that, overall, the free drug showed less toXicity toward the cells, likely because the hydrophobic free drugs failed to solubilize fully and reach the cells, whereas the NP-delivered ARVs were able to enter cells in higher levels and be delivered to the mitochondria. The NPs and polymers themselves were previously shown not to cause cellular toXicity,[18] so it was likely the delivery of the ARVs to the mitochondria that may have caused increased mitochondrial dysfunction and oxidative stress, making the drugs' toxic side effects more visible. Thus, it becomes evident that when ARVs will be delivered with an NP system to hard-to-reach viral reservoirs such as the brain, we need to include a combination therapeutic approach to reduce both the ART- and virus-induced toxic effects such as inflammation and oxidative stress. We evaluated the effects of ARVs on ROS generation and inflammatory marker IL-1β in microglia cells. Treatment with ARVs or ARV-loaded NPs (1 μM of free ARVs or NPs with respect to the loaded drug) increased ROS significantly for the majority of drugs tested, including SQV, EFV, DRV, DTG, or EVG (Figure 3A, Figure S2). Similarly, levels of IL-1β, a marker for inflammation, were seen to increase significantly after treatment with NP-encapsulated ARVs, but not after treatment with the free ARVs (Figure 3B). Our previous studies demonstrated that the empty NPs do not cause any changes in ROS or inflammation.[16] This suggested that the drugs encapsulated in the NPs are effectively targeted to the mitochondria and increased inflammation significantly. Despite the ROS and inflammation generated by the T-ARV-NPs due to their ability to deliver drugs intracellularly, the T-ARV-NPs still remain a more reasonable treatment option over free ARVs, particularly for treatment of HIV in the brain, as the free ARTs have limited ability to cross the BBB to reduce/eliminate CNS HIV reservoirs. As much of the T-ARV-NPs' toxicity is likely due to higher rates of intracellular drug delivery as compared to the relatively insoluble and hydrophobic ARVs, this will likely allow for lower doses of T-ARV-NPs to be used compared to the free ARVs. We then used two drugs of abuse, cocaine and meth, to understand how these drugs alter mitochondrial functions in microglia cells. Seahorse MitoStress assay data suggested that both cocaine and meth at 500 μM substantially decreased indicators of mitochondrial health, including basal and maximal respiration as well as ATP production (Figure 3C,D). The effects of cocaine and meth on human astrocytes were also followed by a MitoStress assay under similar conditions, and the data are presented in Figure S3. These data suggested that the damage to mitochondrial respiration and functions caused by drugs of abuse will likely worsen the effects of any ROS and inflammation caused by treatment with antiretroviral agents in HIV-positive patients. To tackle this issue, combination therapy of BBB-penetrating, mitochondria-targeted NPs loaded with a prodrug of aspirin, Oc-[G2]-$(Asp)_4$, an anti-inflammatory agent, and CoQ_{10}, an antioxidant, could be used to supplement T-ARV-NP treatment in the HIV-positive patient, which likely decrease inflammation and oxidative stress. For all our further studies, we used meth to model the effects of drugs of abuse.

In Vivo Distribution of T-ARV-NPs.

We used female BALB/c albino mice to understand the distribution properties of T-ARV-NPs after intravenous administration. The animals were divided into the following seven groups: saline, EFV, DRV, EVG, T-EFV-NP, T-DRV-NP, and T-EVG-NP. The dose of NP was 40 mg/kg with respect to the drug. After 24 h, around 200 μL of blood was collected in heparinized tubes *via* cardiac puncture. The collected blood was centrifuged to isolate blood plasma. The animals were perfused with saline, sacrificed, and the major organs were harvested, weighed, and digested. The biodistribution was followed by running the samples through HPLC to calculate the percentage of NPs in the organs and blood. This study indicated that the targeted, ARV-loaded NPs were able to cross the blood–brain barrier in significantly higher amounts than the free drug (Figure 4A–C, top). This is a crucial factor in ensuring enough of the drug is delivered across the BBB to effectively treat HIV-infected cells. The drugs were also found to circulate significantly more amounts in the blood when delivered with the NPs (Figure 4A–C, top), indicating a higher possibility of further accumulation in the brain as time progresses. Further, we observed that delivery using the NP system did not cause any significant increase in the liver accumulation of the ARVs compared with the free form (Figure 4A–C, bottom). The whole distribution pattern by measuring %ID and %ID/g of tissue is presented in Figure S4. As a whole, there was higher biodistribution and accumulation of the NP-delivered ARVs as compared to the free ARVs, suggesting the NPs are improving the drugs' half-lives in the blood as well as distribution in the brain. In addition, there was no significant hepatotoxicity due to both the free ARVs and T-ARV-NPs, as shown by normal activity of the liver enzymes alanine aminotransferase and aspartate aminotransferase (Figure 4D).

HIV-Induced Inflammation and ROS Are Reversed by T-$(Asp)_4$-NP and T-CoQ_{10}-NP Formulation.

To mimic the treatment of HIV in a patient with a history of drug abuse, a sequence treatment was conducted over the course of 1 week that included microglia exposure to HIV and meth, followed by treatment consisting of EFV or EVG or the NPs and T-$(Asp)_4$/CoQ_{10}-NPs. A schematic of the experimental details is presented in Figure 5A. Complete characterization of Oc-[G2]-$(Asp)_4$-loaded targeted NPs, T-$(Asp)_4$-NPs, and CoQ_{10}-loaded NPs, T-CoQ_{10}-NPs is provided in Figure S5. Our findings indicated the impact of HIV on the inflammatory cytokines and ROS levels of human microglia cells. HIV enhanced the levels of IL-1β, IL-6, and TNF-α. Analyses of inflammatory responses indicated that the combination of T-$(Asp)_4$-NP and T-CoQ_{10}-NPs was able to reduce the inflammatory signals caused by HIV as well as the enhanced levels caused by meth (Figure 5B and C, Figure S6). Similar effects were found when mitochondrial ROS was assessed using Mito-SOX (Figure 5D).

Protection of Microglia from HIV- and Meth-Induced Toxic Effects by T-CoQ_{10}/$(Asp)_4$-NP-Nourished Astrocytes.

Astrocytes play crucial roles to protect neurons and microglia by providing extensive support in terms of structure and metabolic processes during neurodegenerative processes.[22] Relatively more resistance of astrocytes than neurons toward ROS, mitochondrial

dysfunctions, and other environmental damages gives the astrocytes roles to act as natural protectants of neurons.[23] But, when HIV infection and drug abuse trigger mitochondrial dysfunctions in an astrocyte population, that in succession affects neurons and microglia. Thus, if astrocytes can be protected from mitochondrial dysfunctions, there is a possibility of neuronal survival. The targeted NPs that we are using in this work not only cross the BBB but also localize in the astrocytes, and this NP system targets mitochondria with high efficacy.[14,18,21] Our overall goal in the experiment was to study whether this BBB-penetrating NP with abilities to incorporate and deliver mitochondria-acting natural antioxidant CoQ_{10} and the prodrug aspirin to astrocytes will achieve astrocyte-mediated protection against HAND and drug abuse conditions.

We aimed at simulating HIV infection and drug use in patients with the goal of examining astrocyte-mediated protection of microglia by reducing inflammation and oxidative stress in HIV-infected microglia through coculturing them with astrocytes treated with the T-CoQ_{10}/$(Asp)_4$-NPs, rather than directly treating those microglia with the antioxidant and anti-inflammatory nanoparticles (Figure 6A). On day 1, microglia were treated with Mito-GFP, a signaling protein that allows the mitochondria to fluoresce. On day 3, microglia were treated with 200 ng/mL of TAT peptide,[24] to induce HIV infection-like conditions within the cells. On day 5, microglia were exposed to meth to mimic exposure of a patient's CNS to drugs of abuse. On day 6, microglia were exposed to a combination of T-EFV-NP, T-EVG-NP, and T-DRV-NP, to simulate a combination antiretroviral therapy using the BBB-penetrating NPs. On day 7, the microglia were cocultured with astrocytes. Certain experimental groups of these astrocytes were previously treated with the anti-inflammatory and antioxidant agents in NPs, T-$(Asp)_4$-NP and T-CoQ_{10}-NP in concentrations of 10 μM each. On day 8, microglia were sorted (Figure S7) and examined for levels of inflammatory markers (Figure 6B), ATP (Figure 6C), and ROS (Figure 6D). Microglia treated with TAT peptide, meth, and the T-ART-NPs showed a significant increase in the levels of the inflammatory markers IL-1β, IL-6, and TNF-α, and again, this increase occurred regardless of whether the microglia were kept alone or cocultured with untreated astrocytes, indicating the inflammatory nature of the HIV infection, methamphetamine use, and T-ART-NP treatment (Figure 6B). Compared to the control, microglia treated with TAT peptide, meth, and the T-ART-NPs showed a significant reduction in ATP production, both when these were kept alone and cocultured with untreated astrocytes, suggesting the development of critical mitochondrial dysfunction (Figure 6C). However, if those treated microglia were cocultured with astrocytes (abbreviated as AST*) previously treated with the T-$(Asp)_4$-NPs and T-CoQ_{10}-NPs, there was a significant increase in ATP production, back up to levels close to the control's ATP production levels. Once again, compared to the microglia cocultured with untreated astrocytes, a significant reduction in these inflammatory markers was seen once microglia were cocultured with astrocytes previously treated with T-$(Asp)_4$-NPs and T-CoQ_{10}-NPs. The levels of inflammatory markers returned to the levels seen in untreated microglia, suggesting a strong protective and reparative effect of the healthy, treated astrocytes. Levels of mitochondrial ROS were seen to increase significantly upon exposure to HIV, meth, and the T-ART-NPs, with or without the coculturing of untreated astrocytes (Figure 6D). However, upon coculturing with treated astrocytes, the level of superoxide decreased back down to the level of ROS in the control microglia. These results were further supported

through the fluorescence imaging that shows the colocalization of mito-GFP and mito-SOX markers in the mitochondria of treated cells, followed by a decrease in fluorescence in microglia cocultured with treated astrocytes (Figure 7). These results paint a promising picture of therapies that take advantage of astrocyte-mediated protection and repair. Although the specific mechanism by which aspirin- and CoQ_{10}-treated astrocytes modulate a decrease in ROS and inflammation and mitochondrial rejuvenation in HIV-positive, meth-exposed microglia remains unknown, there is a clear improvement in these metrics upon the coculturing with treated astrocytes. This suggests that the potential damage done by HIV infection, drugs, and subsequent therapies can be repaired through cotreatment in the CNS with the nanoparticle-based delivery of antioxidants and anti-inflammatory agents.

In Vivo Evaluation of T-ART-NPs and T-CoQ_{10}/$(Asp)_4$-NPs in EcoHIV-Infected Mice under Methamphetamine Use Conditions.

To evaluate the effectiveness of our combination of BBB-penetrating, antiviral, antioxidant, and anti-inflammatory NPs in a living system, we infected mice with ecotropic HIV (EcoHIV) *via* tail i.v.[25] and subsequently exposed them to meth to emulate patients with substance abuse issues. EcoHIV is a modified form of human HIV by switching gp120 gene which encodes surface by gp80 so that the virus could only infect mice.[26–28] We also injected a control virus, pBMN-I-GFP, to serve as a control for EcoHIV, which does not cause any toxicity or inflammation in the mice. After meth exposure, the mice were treated with a combination T-ART-NP (T-EVG-NP, T-EFV-NP, and T-DRV-NP), followed by treatment with a combination of T-CoQ_{10}-NP and T-$(Asp)_4$-NP. After the experiment was concluded, the mice were sacrificed for *ex vivo* analyses. A detailed timeline and description of this experiment are represented in Figure 8A.

First, levels of HIV viral protein p24 were evaluated from blood plasma and brain tissue lysate through ELISA and RT-PCR, respectively (Figure 8B, Figure S8). In EcoHIV-positive mice exposed to meth, the levels of p24 antigen were elevated, except for those treatment groups that received T-ART-NP; these groups showed a reduction in p24 levels (Figure 8B). This indicates that the T-ART-NPs are highly effective at treating HIV. Further, anti-inflammatory cytokines IL-1β and TNF-α were evaluated in blood plasma through ELISA, and these levels were increased in both EcoHIV-infected and EcoHIV- and meth-exposed mice (Figure 8C). The inflammation was decreased with the treatment of T-CoQ_{10}/$(Asp)_4$-NPs alone and in combination with T-ART-NPs (Figure 8C). RT-PCR was used to evaluate mRNA levels of neuro-inflammation markers C3 and OLFM1 in brain lysates (Figure 8D). EcoHIV-infected mice showed a rise in neuroinflammation, which was decreased after the treatment of T-CoQ_{10}/$(Asp)_4$-NPs alone and in combination with T-ART-NPs (Figure 8D). Glutamate-cysteine ligase catalytic subunit (GCLC) and glutamate-cysteine ligase modifier subunit (GCLM) are the enzymes that are involved in glutathione synthesis to control the elevated ROS level. Glutathione peroxidase 7 (GPX7) is a member of the glutathione peroxidase family that regulates ROS. Using RT-PCR analyses, we measured the mRNA levels of the ROS markers GCLC, GCLM, and GPX7 (Figure 8E). The data revealed that mice infected with EcoHIV and exposed to meth had high levels of ROS and treatment with T-ART-NPs did not cause any changes in the ROS. When treated with the T-CoQ_{10}/$(Asp)_4$-NPs, there was a reduction in these levels, indicating the NPs are effective

at reducing oxidative stress caused by substance abuse along with EcoHIV infection (Figure 8E). Overall, the combination of T-ART-NPs and T-CoQ_{10}/$(Asp)_4$-NPs is able to control the neuroinflammation and the ROS levels in the brain caused by EcoHIV infection.

We also evaluated the ROS levels in glial cells and neurons that were isolated from freshly harvested brain samples and grown in their respective selective media. The ROS level was increased in astrocytes and neurons from EcoHIV-infected mice and reduced in the mice that were treated with the T-CoQ_{10}/$(Asp)_4$-NPs (Figure 9A). The isolated cells were characterized with GFAP and NeuN marker for astrocytes and neurons, respectively (Figure S9). Immunofluorescence was performed on brain tissue samples to study the site of accumulation of the viral particle. The samples were stained for p24 viral protein along with GFAP for astrocytes (Figure S10), MAP2 for neurons (Figure S11), TMEM119 for microglia (Figure S12), ICAM-1 for the signaling factor involved in neuroinflammation (Figure S13), and catalase for the ROS marker (Figure S14). These data indicated that treatment using the T-ART-NPs and T-CoQ_{10}/$(Asp)_4$-NPs showed reduction in HIV infection in the brain, levels of inflammation, and oxidative stress (Figures S10–S14). H&E staining was conducted to observe tissue damage in all organs, which did not reveal any structural toxicity (Figure 9B, Figure S15). One of the significant aspects of this study is the ability of the NPs to effectively accumulate in the brain. This property leads to an increased bioavailability of the ARVs in the viral reservoirs of the brain, which is difficult to achieve with the free form of the ARVs. With this platform we are able to deliver various classes of antiviral drugs to the brain. In addition, the combination of these ARV-loaded NPs along with T-CoQ_{10}/$(Asp)_4$-NPs was also able to lower the neuroinflammation and ROS levels caused by EcoHIV and a drug of abuse. Taken together, these studies revealed that combination therapy with the nanoparticles could result in a highly effective treatment regimen for the HIV-infected population who are addicted to a substance of abuse.

CONCLUSIONS

In this work, we combined a lipophilic, biodegradable, brain-accumulating, intracellular-targeted NP containing ARVs with NPs containing antioxidants and anti-inflammatory agents to treat HIV infection in a model of HIV infection and recreational drug use. This work is based on a combination of synergizing conceptual and technical innovations to gain an understanding of the effectiveness of combination therapy and future clinical translation. In particular, this work provides a platform to (a) obtain knowledge on the effects of brain-accumulating NPs containing ARVs, antioxidants, and anti-inflammatory agents on the HIV-infected population; (b) utilize the inherently hyperpolarized mitochondria of astrocytes and microglia to target these cell populations using the brain-penetrating NP system containing mitochondria-acting antioxidant and anti-inflammatory drugs; (c) deliver an antioxidant inside the mitochondrial lumen where dysfunctions and ROS are located; (d) simultaneously deliver an anti-inflammatory agent; (e) astrocyte and microglia assisted neuron protection, and viral load reduction in the brain; and (f) develop the biodegradable NP used in this study from a single-step, controlled procedure that produces NPs with distinct properties. In synthesizing the nanoparticles, all chemical conjugations occur before NP formulation from the polymers, which minimizes variability. In addition, through an extensive study in a mice model of HIV infection and drug abuse, the combination nanoparticle treatment was

shown to be effective in reducing HIV infection, inflammation, and oxidative stress. This approach is robust, simple in design, and scalable, making it well suited for potential clinical translation.

EXPERIMENTAL SECTION

Statistics.

All data were expressed as mean ± SD (standard deviation). GraphPad Prism software v. 5.00 was used to perform all statistical analyses. An unpaired Student's *t* test was performed to make comparisons between two values. A one-way ANOVA with a *posthoc* Tukey test was used to identify significant differences among the groups. The two-tailed statistical analyses were conducted at significance level $P = 0.05$.

Materials and Methods.

Materials and methods are described in the Supporting Information.

Animals.

Balb/c albino female mice (4–8 weeks old) and C57BL/6 male mice (13 weeks old) were purchased from Jackson Laboratory. All animals were handled in accordance with "The Guide for the Care and Use of Laboratory Animals" of the American Association for Accreditation of Laboratory Animal Care (AAALAC), Animal Welfare Act (AWA), and other applicable federal and state guidelines. All animal work presented here was approved by the Institutional Animal Care and Use Committee (IACUC) of University of Miami (UM) Miller School of Medicine. All housing, surgical procedures, and experimental protocols were approved by the IACUC Committee of UM. Animals had free access to chow diet and water during all experiments.

Supplementary Material

Refer to Web version on PubMed Central for supplementary material.

Acknowledgments

This work was supported by the Sylvester Comprehensive Cancer Center and the NCI funded Sylvester Comprehensive Cancer Center support grant 1P30CA240139, University of Miami Miller School of Medicine, to S.D; H&N Wertheim Research Pilot Project from Florida International University and the Institute of NeuroImmune Pharmacology to N.K.; the National Institutes of Health (NIH) grants DA044579 and DA050528 to M.T.; and NIH grants DA042706, DA040537, DA037838, and DA034547 to M.N. We thank Dr. Atluri and Ms. Adriana Yndart Arias for their help with the propagation of HIV-1.

REFERENCES

(1). Fauci AS The AIDS Epidemic-Considerations for the 21st Century. N. Engl. J. Med 1999, 341, 1046–1050. [PubMed: 10502595]

(2). Piot P; Bartos M; Ghys PD; Walker N; Schwartlander B The Global Impact of HIV/AIDS. Nature 2001, 410, 968–973. [PubMed: 11309626]

(3). Antinori A; Arendt G; Becker JT; Brew BJ; Byrd DA; Cherner M; Clifford DB; Cinque P; Epstein LG; Goodkin K; Gisslen M; Grant I; Heaton RK; Joseph J; Marder K; Marra CM; McArthur

JC; Nunn M; Price RW; Sacktor VV; et al. Updated Research Nosology for HIV-Associated Neurocognitive Disorders. Neurology 2007, 69, 1789–1799. [PubMed: 17914061]

(4). Saylor D; Dickens AM; Sacktor N; Haughey N; Slusher B; Pletnikov M; Mankowski JL; Brown A; Volsky DJ; McArthur JC HIV-Associated Neurocognitive Disorder-Pathogenesis and Prospects for Treatment. Nat. Rev. Neurol 2016, 12, 234–248. [PubMed: 26965674]

(5). Brabers NA; Nottet HS Role of the Pro-Inflammatory Cytokines TNF-alpha and IL-1beta in HIV-Associated Dementia. Eur. J. Clin. Invest 2006, 36, 447–458. [PubMed: 16796601]

(6). Akay C; Lindl KA; Shyam N; Nabet B; Goenaga-Vazquez Y; Ruzbarsky J; Wang Y; Kolson DL; Jordan-Sciutto KL Activation Status of Integrated Stress Response Pathways in Neurones and Astrocytes of HIV-Associated Neurocognitive Disorders (HAND) Cortex. Neuropathol. Appl. Neurobiol 2012, 38, 175–200. [PubMed: 21883374]

(7). Dutta R; Roy S Mechanism(s) Involved in Opioid Drug Abuse Modulation of HAND. Curr. HIV Res 2012, 10, 469–477. [PubMed: 22591371]

(8). Sanchez AB; Kaul M Neuronal Stress and Injury Caused by HIV-1, cART and Drug Abuse: Converging Contributions to HAND. Brain Sci 2017, 7, 1–22.

(9). Hazleton JE; Berman JW; Eugenin EA Novel Mechanisms of Central Nervous System Damage in HIV Infection. HIV/AIDS 2010, 2, 39–49.

(10). Lindl KA; Marks DR; Kolson DL; Jordan-Sciutto KL HIV-Associated Neurocognitive Disorder: Pathogenesis and Therapeutic Opportunities. J. Neuroimmune Pharmacol 2010, 5, 294–309. [PubMed: 20396973]

(11). Ton H; Xiong H Astrocyte Dysfunctions and HIV-1 Neurotoxicity. J. AIDS Clin. Res 2013, 4, 255–267. [PubMed: 24587966]

(12). Zayyad Z; Spudich S Neuropathogenesis of HIV: From Initial Neuroinvasion to HIV-Associated Neurocognitive Disorder (HAND). Curr. HIV/AIDS Rep 2015, 12, 16–24. [PubMed: 25604237]

(13). Kaul M; Garden GA; Lipton SA Pathways to Neuronal Injury and Apoptosis in HIV-Associated Dementia. Nature 2001, 410, 988–994. [PubMed: 11309629]

(14). Surnar B; Basu U; Banik B; Ahmad A; Marples B; Kolishetti N; Dhar S Nanotechnology-Mediated Crossing of Two Impermeable Membranes to Modulate the Stars of the Neurovascular Unit for Neuroprotection. Proc. Natl. Acad. Sci. U. S. A 2018, 115, E12333–E12342. [PubMed: 30530697]

(15). Velichkovska M; Surnar B; Nair M; Dhar S; Toborek M Targeted Mitochondrial CoQ10 Delivery Attenuates Antiretroviral Drug-Induced Senescence of Neural Progenitor Cells. Mol. Pharmaceutics 2019, 16, 724–736.

(16). Kalathil AA; Kumar A; Banik B; Ruiter TA; Pathak RK; Dhar S New Formulation of Old Aspirin for Better Delivery. Chem. Commun 2016, 52, 140–143.

(17). Feldhaeusser B; Platt SR; Marrache S; Kolishetti N; Pathak RK; Montgomery DJ; Reno LR; Howerth E; Dhar S Evaluation of Nanoparticle Delivered Cisplatin in Beagles. Nanoscale 2015, 7, 13822–13830. [PubMed: 26234400]

(18). Marrache S; Pathak RK; Dhar S Detouring of Cisplatin to Access Mitochondrial Genome for Overcoming Resistance. Proc. Natl. Acad. Sci. U. S. A 2014, 111, 10444–10449. [PubMed: 25002500]

(19). Marrache S; Tundup S; Harn DA; Dhar S Ex Vivo Programming of Dendritic Cells by Mitochondria-Targeted Nanoparticles to Produce Interferon-Gamma for Cancer Immunotherapy. ACS Nano 2013, 7, 7392–7402. [PubMed: 23899410]

(20). Hung SW; Mody H; Marrache S; Bhutia YD; Davis F; Cho JH; Zastre J; Dhar S; Chu CK; Govindarajan R Pharmacological Reversal of Histone Methylation Presensitizes Pancreatic Cancer Cells to Nucleoside Drugs: In Vitro Optimization and Novel Nanoparticle Delivery Studies. PLoS One 2013, 8, e71196–e71199. [PubMed: 23940717]

(21). Marrache S; Dhar S Engineering of Blended Nanoparticle Platform for Delivery of Mitochondria-Acting Therapeutics. Proc. Natl. Acad. Sci. U. S. A 2012, 109, 16288–16293. [PubMed: 22991470]

(22). Chen Y; Swanson RA Astrocytes and Brain Injury. J. Cereb. Blood Flow Metab 2003, 23, 137–149. [PubMed: 12571445]

(23). Voloboueva LA; Suh SW; Swanson RA; Giffard RG Inhibition of Mitochondrial Function in Astrocytes: Implications for Neuroprotection. J. Neurochem 2007, 102, 1383–1394. [PubMed: 17488276]

(24). Samikkannu T; Rao KV; Kanthikeel SP; Atluri VS; Agudelo M; Roy U; Nair MP Immunoneuropathogenesis of HIV-1 Clades B and C: Role of Redox Expression and Thiol Modification. Free Radical Biol. Med 2014, 69, 136–144. [PubMed: 24480751]

(25). Geraghty P; Hadas E; Kim B-H; Dabo AJ; Volsky DJ; Foronjy R HIV Infection Model of Chronic Obstructive Pulmonary Disease in Mice. Am. J. Physiol. Lung Cell Mol 2017, 312, L500–L509.

(26). Gu C-J; Borjabad A; Hadas E; Kelschenbach J; Kim B-H; Chao W; Arancio O; Suh J; Polsky B; McMillan J; Edagwa B; Gendelman HE; Potash MJ; Volsky DJ EcoHIV Infection of Mice Establishes Latent Viral Reservoirs in T Cells and Active Viral Reservoirs in Macrophages that are Sufficient for Induction of Neurocognitive Impairment. PLoS Pathog 2018, 14, e1007061–e1007061. [PubMed: 29879225]

(27). Jones LD; Jackson JW; Maggirwar SB Modeling HIV-1 Induced Neuroinflammation in Mice: Role of Platelets in Mediating Blood-Brain Barrier Dysfunction. PLoS One 2016, 11, e0151702–e0151709. [PubMed: 26986758]

(28). Spire B; Sire J; Zachar V; Rey F; Barré-Sinoussi F; Galibert F; Hampe A; Chermann J-C Nucleotide Sequence of HIV1-NDK: a Highly Cytopathic Strain of the Human Immunodeficiency Virus. Gene 1989, 81, 275–284. [PubMed: 2806917]

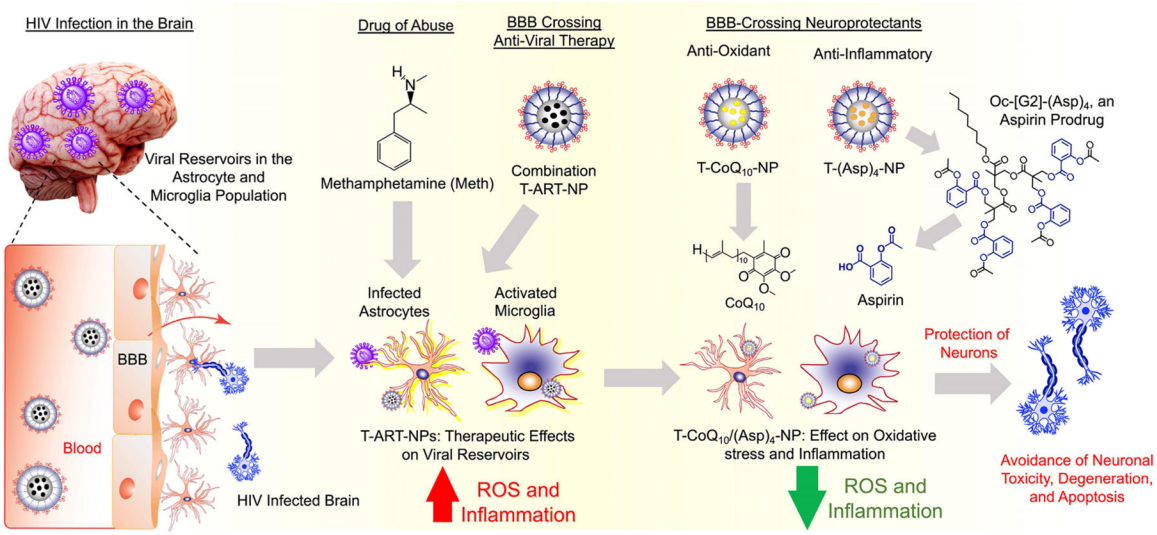

Figure 1.

BBB-penetrating T-NPs containing ARVs, antioxidant CoQ_{10}, and a prodrug of aspirin, Oc-[G2]-$(Asp)_4$, for improvement of mitochondrial functions and reduction of inflammation in astrocytes and microglia to promote neuronal protection in HIV-infected brain under drug abuse conditions.

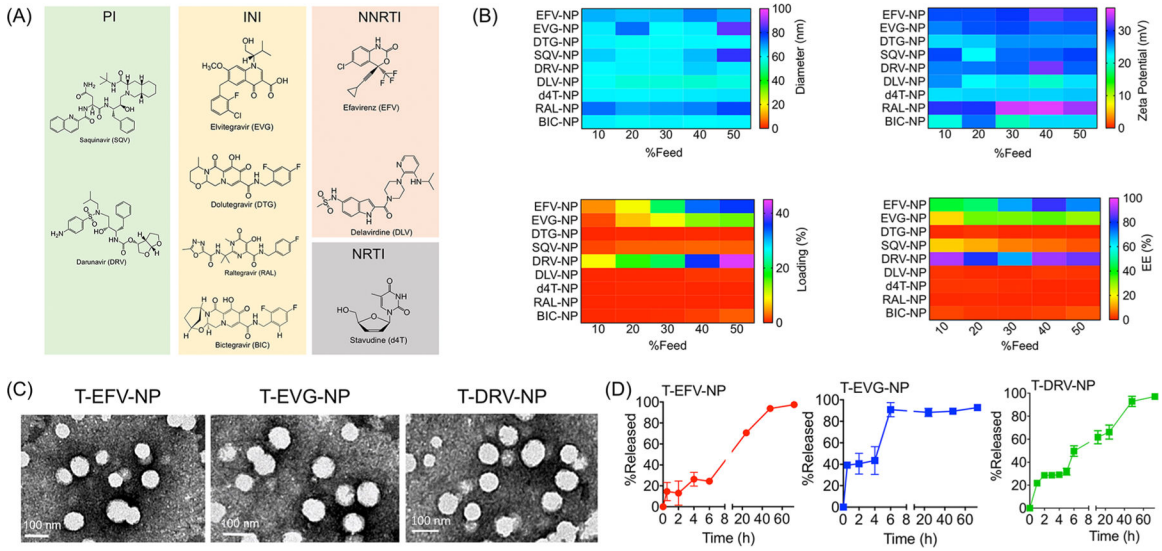

Figure 2.

(A) Structures of ARVs investigated for inclusion in the core of targeted NPs, along with their classification based on molecular target: protease inhibitor (PI), integrase inhibitor (INI), nucleoside/nucleotide reverse transcriptase inhibitor (NRTI), and non-nucleoside reverse transcriptase inhibitor (NNRTI). (B) Heat maps for diameter, zeta potential, percent loading, and percent encapsulation efficiency of ARV-loaded NPs. (C) TEM images of T-EFV-NP, T-EVG-NP, and T-DRV-NP. (D) Release profiles of EFV, EVG, and DRV from T-NPs at pH 7.4 at 37 °C.

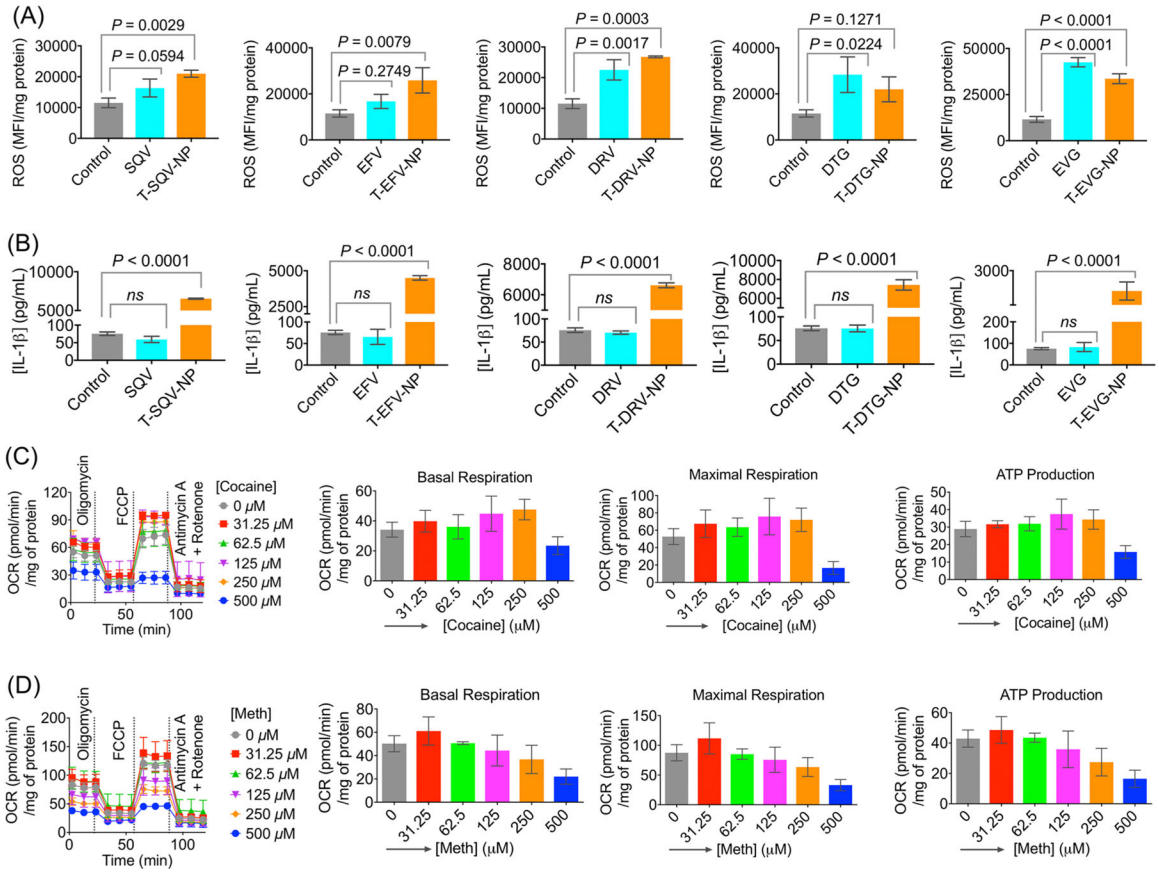

Figure 3.

(A) Elevated intracellular ROS levels in microglia cells treated with SQV, EFV, DRV, DTG, EVG, or the nanoformulations T-SQV-NP, T-EFV-NP, T-DRV-NP, T-DTG-NP, and T-EVG-NP at a concentration of 1.0 μM for 24 h. (B) Inflammatory responses by the microglia cells by measuring the excretion of IL-1β in the media when these cells were treated with SQV, EFV, DRV, DTG, EVG, or the nanoformulations T-SQV-NP, T-EFV-NP, T-DRV-NP, T-DTG-NP, and T-EVG-NP at a concentration of 1.0 μM for 24 h. Effects of (C) cocaine and (D) meth on mitochondrial basal respiration, maximal respiration, and ATP production as determined by Seahorse MitoStress analyses in microglia cells. The abuse drug concentration was varied from 0 to 500 μM, and cells were treated for 24 h.

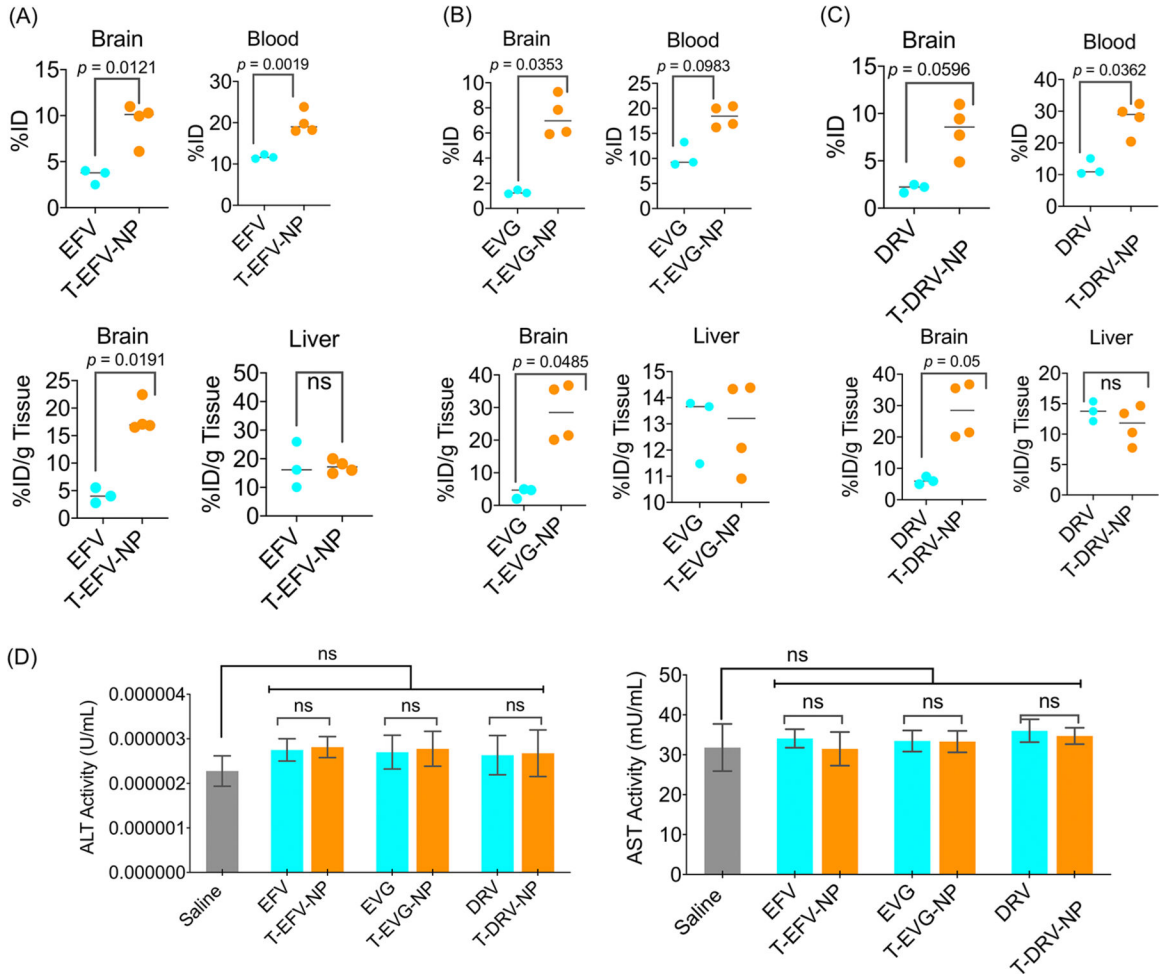

Figure 4.

In vivo distribution of intravenously injected T-ARV-NPs in the brain, liver, and blood of female Balb/c mice for (A) EFV and T-EFV-NP, (B) EVG and T-EVG-NP, and (C) DRV and T-DRV-NP. (D) Alanine aminotransferase (ALT) and aspartate aminotransferase (AST) levels in the blood plasma. The animals were dosed with 40 mg/kg with respect to the ARVs.

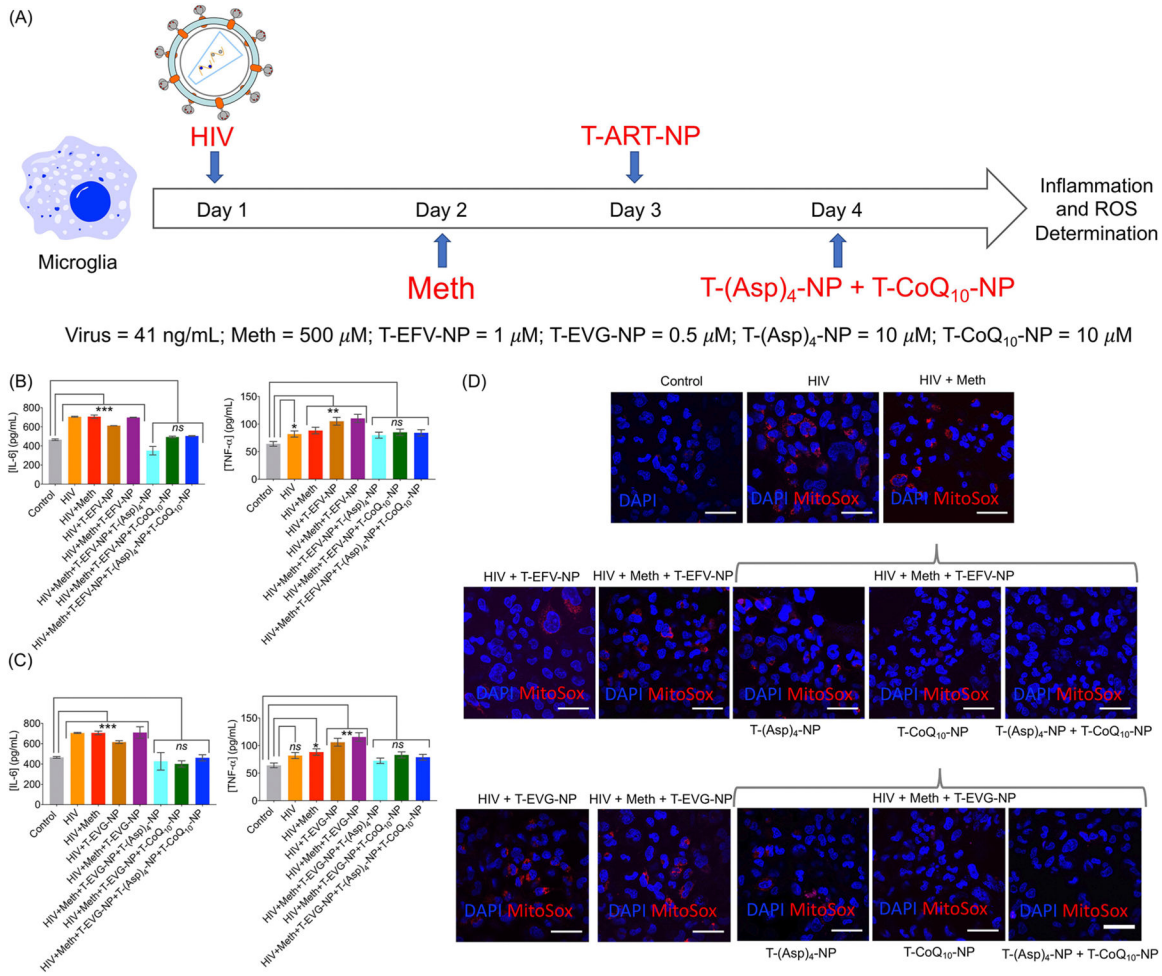

Figure 5.

(A) Timeline showing the experimental details of HIV-induced generation of inflammatory and ROS responses in microglia is reversed by T-$(Asp)_4$-NP and T-CoQ_{10}-NP formulations. HIV-infected human microglia cells were treated with meth to elevate the responses further. The cells were then treated with T-EVG-NP or T-EFV-NP and then treated with T-$(Asp)_4$-NP and T-CoQ_{10}-NP. Inflammatory responses by analyzing IL-6 and TNF-α (B) in the presence of T-EFV-NP and (C) in the presence of T-EVG-NP. (D) Reversal of mitochondrial oxidative stress by the Mito-SOX assay from the experiment detailed in (A). Scale bar = 50 μm. For IL-6: *** = 0.0003; ** = 0.0022; * = 0.0252. For TNF-α: *** = 0.0005; ** = 0.0039; * = 0.0158.

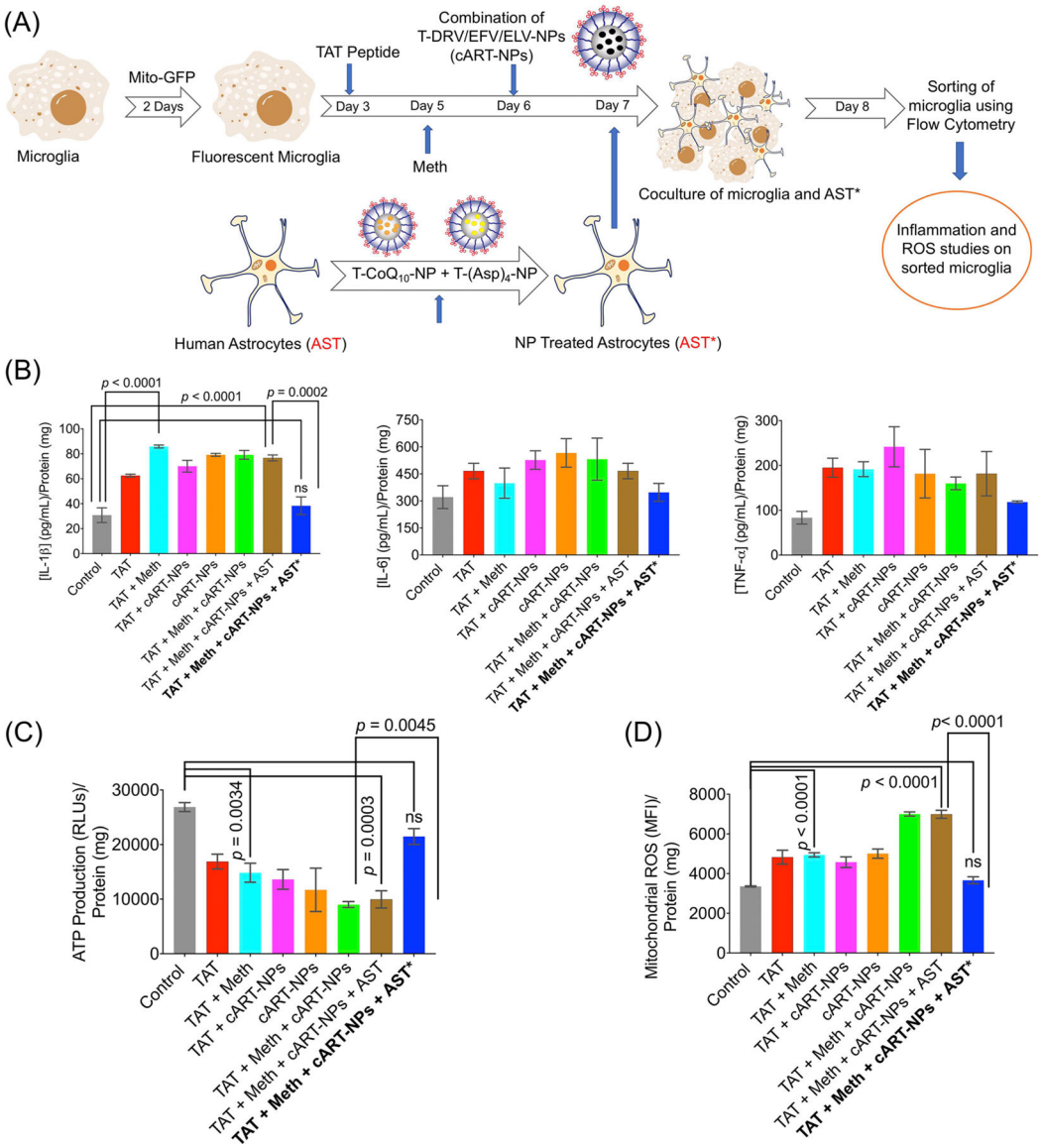

Figure 6.

(A) Schematic of the experimental approach where microglia cells were fluorescently labeled with mito-GFP, followed by treatment with TAT peptide, methamphetamine, and a combination of T-DRV/EFV/ELV-NP. These microglia cells were then cocultured with astrocytes treated with a combination of T-$(Asp)_4$-NP + T-CoQ_{10}-NP. (B) Cellular levels of the inflammatory markers IL-1β, IL-6, and TNF-α in microglia after coculturing with NP-treated astrocytes. (C) ATP levels and (D) ROS levels in microglia after nourishing with astrocytes. AST: human astrocyte; AST*: neuroprotectant-loaded-NP-treated human astrocytes.

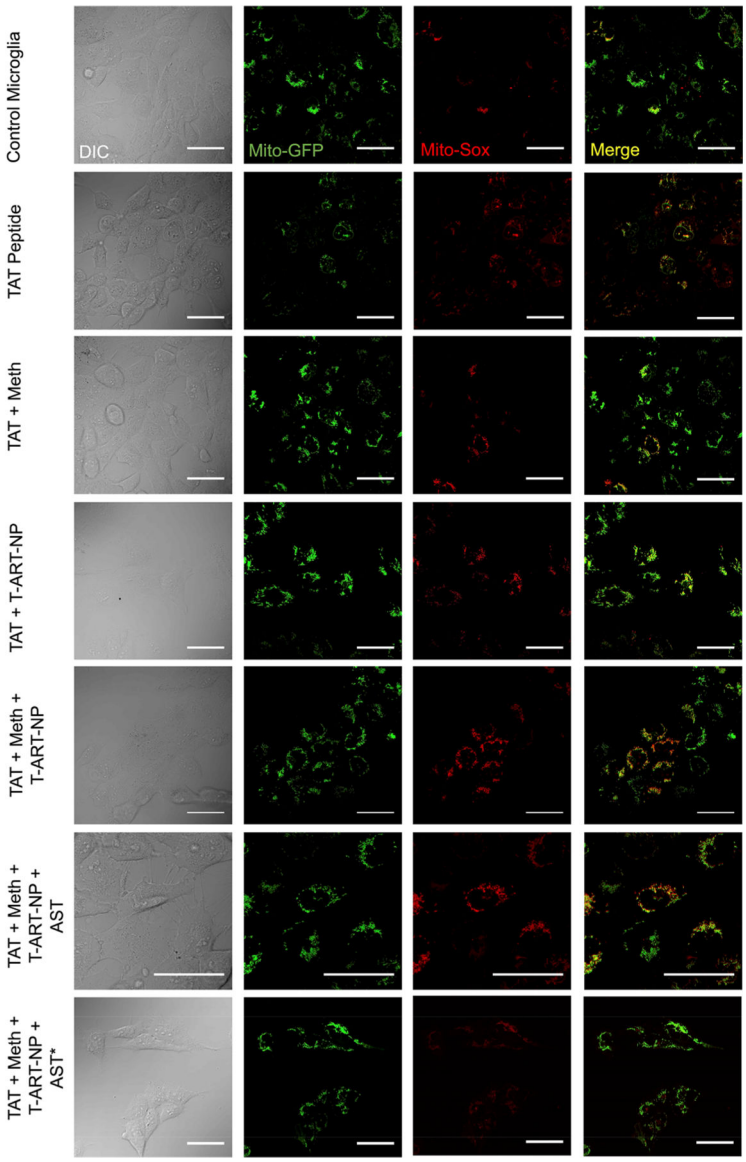

Figure 7.

Determination of mitochondrial ROS using fluorescently labeled microglia cells that were treated with TAT peptide, methamphetamine, and a combination of T-DRV/EFV/ELV-NP, followed by coculture with astrocytes that were treated with a combination of T-$(Asp)_4$-NP+ T-CoQ_{10}-NP (scale bar = 50 μm).

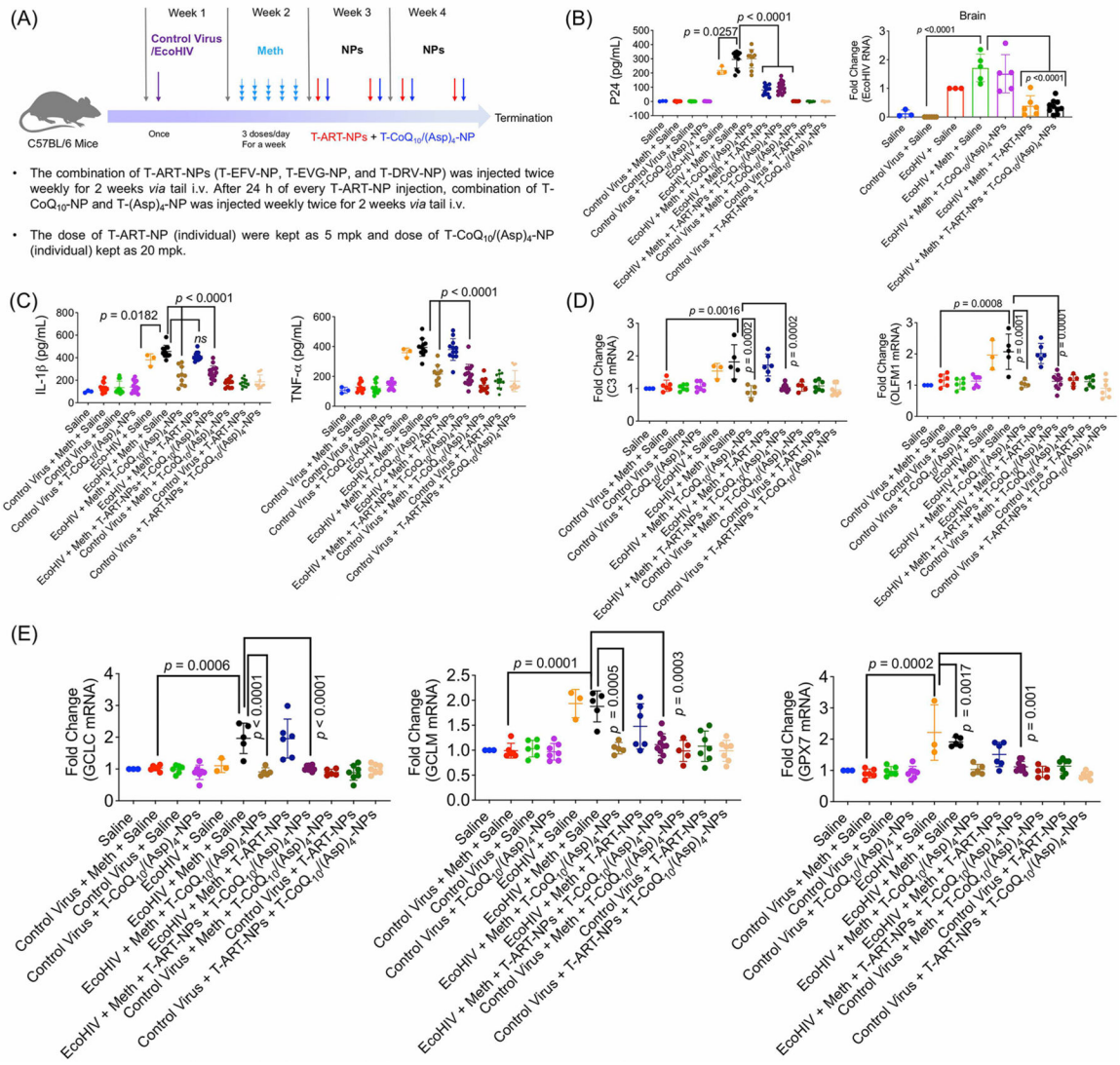

Figure 8.

Efficacy studies in an EcoHIV-infected meth-treated animal model. C57BL/6 male mice were divided into 12 groups and were assigned to the following treatment groups: control virus + meth + saline (12 animals); control virus + saline (12 animals); control virus + meth + T-CoQ_{10}-NP/T-$(Asp)_4$-NP (13 animals); EcoHIV + meth + saline (11 animals); EcoHIV + meth + T-CoQ_{10}-NP/T-$(Asp)_4$-NP (10 animals); EcoHIV + meth + T-ART-NPs (12 animals); EcoHIV + meth + T-ART-NP + T-CoQ_{10}-NP/T-$(Asp)_4$-NP (16 animals); control virus + meth + T-CoQ_{10}/$(Asp)_4$-NPs (11 animals); control virus + T-ART-NPs (13 animals); control virus + T-ART-NPs + T-CoQ_{10}/$(Asp)_4$-NPs (12 animals), saline (3 animals), and EcoHIV + saline (3 animals). (A) Timeline illustrating infection of C57BL/6 male mice with either control virus (pBMN-I-GFP) or chimeric HIV-NDK (EcoHIV, 1 μg of p24), followed by one-week multiday exposure to meth (0.2 mg/kg at each injection for 5 days) and subsequent two-week treatment with T-ART-NPs (5 mg/kg with respect to the drug) and T-CoQ_{10}/$(Asp)_4$-NPs (20 mg/kg with respect to the drug). (B) Levels of EcoHIV p24 antigen in blood by ELISA and in the brain by RT-PCR. (C) Inflammatory markers

IL-1β and TNF-α as measured by ELISA in blood plasma. (D) Neuroinflammation markers C3 and OLFM1 measured by RT-PCR in the brain. (E) ROS markers glutamate-cysteine ligase catalytic subunit (GCLC), glutamate-cysteine ligase modifier subunit (GCLM), and glutathione peroxidase 7 (GPX7) were measured using RT-PCR in the brain.

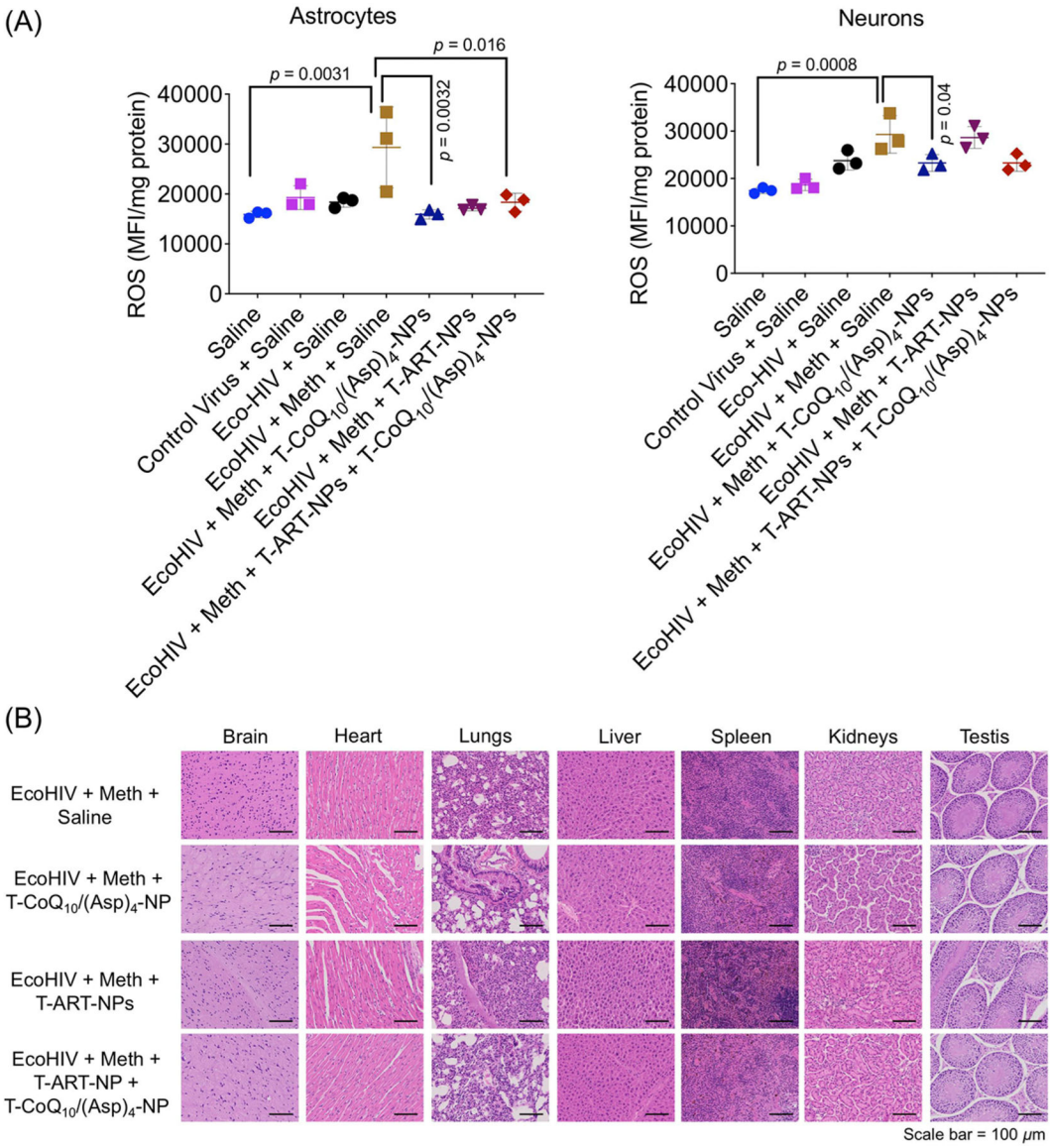

Figure 9.

(A) ROS levels in isolated astrocytes and neurons from treated mice brain. (B) H&E images of all the tissue sections after the treatment (scale bar = 50 μm). C57BL/6 male mice were divided into 12 groups and were assigned to the following treatment groups: control virus + meth + saline (12 animals); control virus + saline (12 animals); control virus + meth + T-CoQ_{10}-NP/T-$(Asp)_4$-NP (13 animals); EcoHIV + meth + saline (11 animals); EcoHIV + meth + T-CoQ_{10}-NP/T-$(Asp)_4$-NP (10 animals); EcoHIV + meth + T-ART-NPs (12 animals); EcoHIV + meth + T-ART-NP + T-CoQ_{10}-NP/T-$(Asp)_4$-NP (16 animals); control virus + meth + T-CoQ_{10}/$(Asp)_4$-NPs (11 animals); control virus + T-ART-NPs (13 animals); control Virus + T-ART-NPs + T-CoQ_{10}/$(Asp)_4$-NPs (12 animals), saline (3 animals), and EcoHIV + saline (3 animals). The mice were treated with either control virus (pBMN-I-GFP) or chimeric HIV-NDK (EcoHIV, 1 μg of p24), followed by one-week multiday exposure to meth (0.2 mg/kg at each injection for 5 days) and subsequent two-week treatment with

T-ART-NPs (5 mg/kg with respect to the drug) and T-CoQ_{10}/$(Asp)_4$-NPs (20 mg/kg with respect to the drug) *via* an intravenous route

Table 1.

Summary of ARVs Used for Optimization and Characterization of Drug-Loaded NPs

SI. No.	ARV	Abbreviation	Activity	Diameter (nm)	Zeta Potential (mV)	%Loading	%EE
1	**Saquinavir**	**sQv**	**PI**	**56±1.8**	**21±1.9**	**1.5±2.1**	**14.8±42.0**
2	Atazanavir	ATV	PI	60±2.6	25±0.8	ND	ND
3	Tenofovir	TDF	NRTI	58±2.3	22±0.3	ND	ND
4	Indinavir	IDV	PI	56±2.8	20±1.8	ND	ND
5	Ritonavir	RTV	PI	58±1.2	26±1.2	ND	ND
6	Zidovudine	ZDV	NRTI	56±1.2	24±0.5	ND	ND
7	Lopinavir	LPV	PI	58±1.9	24±0.1	ND	ND
8	**Efavirenz**	**EFV**	**NNRTI**	**59±1.6**	**20±0.9**	**4.2±1.9**	**42±2.0**
9	**Darunavir**	**DRV**	**PI**	**58±1.5**	**21±10.3**	**8.3±2.0**	**83±2.0**
10	Nevirapine	NVP	NNRTI	55±0.8	26±0.6	ND	ND
11	Lamivudine	3TC	NRTI	62±1.7	25±0.3	ND	ND
12	Fosamprenavir	FPV	Pl	55±1.7	23±2.5	ND	ND
13	Amprenavir	APV	PI	57±2.0	24±2.3	ND	ND
14	**Dolutegravir**	**DTG**	**INI**	**60±8.5**	**24±1.4**	**0.13±0.8**	**1.3±0.9**
15	**Elvitegravir**	**EVG**	**INI**	**58±1.4**	**23±0.6**	**1.8±2.0**	**18.2±2.5**
16	Cobicistat	CcosBl	PK Enhancer	70±2.1	27±0.8	ND	ND
17	Abacavir	ABC	NRTI	57±1.7	23±4.2	ND	ND
18	Emtricitabine	FTC	NRTI	56±1.4	24±2.1	ND	ND
19	**Raltegravir**	**RAL**	**INI**	**65±1.8**	**26±0.5**	**0.07±0.01**	**0.8±0.8**
20	Maraviroc	MVC	CCRS5 Inhibitor	65±2.4	24±0.5	ND	ND
21	Enfuvirtide	T20	Fusion Inhibitor	60±1.9	22±14	ND	ND
22	**Delavirdine**	**DLV**	**NNRTI**	**56±1.4**	**19±0.8**	**0.74±1.0**	**7.4±1.2**
23	**Bictegravir**	**BIC**	**INI**	**57±1.4**	**29±1.4**	**0.48±0.9**	**4.9±1.2**
24	Didanosine	ddl	NRTI	56±1.8	20±1.8	ND	ND
25	Zalcitabine	ddc	NRTI	62±1.7	22±2.3	ND	ND
26	**Stavudine**	**d4T**	**NRTI**	**58±2.9**	**21±1.4**	**0.26±0.2**	**2.6±1.0**

PI: Protease Inhibitor

INI: Integrase inhibitors

NRTI: Nucleoside/Nucleotide Reverse Transcriptase Inhibitors

NNRTI: Non-nucleoside reverse transcriptase inhibitors

ND: Not detectable by HPLC